Electron paramagnetic resonance study of Eu^{2+} centers in melt-grown CsBr single crystals

H. Vrielinck,[a] D. G. Zverev,[a,b], P. Leblans,[c] J.-P. Tahon,[c] P. Matthys[a] and F. Callens[a]

a) Ghent University, Department of Solid State Sciences, Krijgslaan 281-S1, B-9000 Gent, Belgium

b) Max Planck Institute for Polymer Research, Ackermannweg 10, D-55128 Mainz, Germany

c) Agfa-HealthCare NV, Septestraat 27, B-2640 Mortsel, Belgium

Abstract

The structure of Eu^{2+} monomer centers in CsBr single crystals is investigated using electron paramagnetic resonance (EPR) spectroscopy. These centers are produced by heating the melt-grown crystals above 600 K in vacuum followed by a rapid quench to room temperature (RT) or 77 K. The angular dependence of their EPR spectrum demonstrates that these centers have cubic symmetry. At RT the EPR spectrum decays by aggregation of the Eu^{2+} ions. This strongly contrasts with the situation for CsBr:Eu Needle Image Plates synthesized by physical vapor deposition, where the Eu^{2+}-related EPR spectrum was observed to exhibit long-term stability at RT.

PACS numbers : 87.59.bd, 76.30.Kg, 78.60.Lc

Corresponding author :
Henk Vrielinck, Ghent University–Department of Solid State Sciences,
Krijgslaan 281-S1, B-9000 Gent, Belgium.
Tel. : +32 9 264 43 56. FAX : +32 9 264 49 96
Henk.Vrielinck@UGent.be

I. Introduction

It is well known that in alkali halides (AX) many divalent cations (M^{2+}) aggregate at ambient temperature, these include Pb^{2+},[1,2] the transition metal ions Mn^{2+} [3,4] and Fe^{2+},[5] and the rare-earth ions Sm^{2+}, Eu^{2+} and Yb^{2+}.[6,7] Very often, these divalent ions have a cation vacancy (V_A) in their direct vicinity which preserves charge compensation. Attraction between the electric dipoles $M^{2+}{}_A$–V_A is considered to be the driving force for the aggregation, while vacancies assure the mobility of the impurity ions. In many cases, the initial decay kinetics of the dipole monomer centers were observed to be of third order, suggesting the formation of $M^{2+}{}_A$–V_A trimers as a first step in the aggregation process.[3,7] Direct trimer formation seems very unlikely, in view of the low probability of coincidence for three $M^{2+}{}_A$–V_A dipoles. However, Crawford demonstrated that a monomer dipole decay proportional to the third power of the monomer concentration is observed if trimers are formed by capture of dipole monomers by dimers, in which the monomers exhibit low binding energy.[8] For many M^{2+} impurity – AX host combinations the location of the V_A could be determined from the symmetry of the defect, as established from angular dependent electron paramagnetic resonance (EPR) studies on single crystals. Such experiments demonstrated that several vacancy configurations may coexist and that charge compensation of divalent substitutional impurities in alkali halides is not necessarily local (see e.g. also Rh^{2+} in NaCl[9,10] and AgCl[11]).

Among these systems, CsBr:Eu has regained interest in the past decade. Since the late 1990's research efforts have been directed towards the development of a CsBr:Eu^{2+} based X-ray storage phosphor for medical image plates (IPs) in computer radiography, that would solve the resolution problems of the BaFBr:Eu^{2+} powder IPs, while maintaining high sensitivity. It was found that thermal evaporation of CsBr:Eu^{2+} on an Al substrate may result in oriented needle growth (needle image plate, NIP), with needles only a few µm in diameter and up to several 100 µm in length, matching resolution and sensitivity requirements.[12-14] This in itself is quite remarkable, as melt-grown Eu^{2+} doped single crystals perform rather poorly as photo-stimulated luminescence (PSL) phosphors. Our EPR investigation of NIPs demonstrated that they exhibit a Eu^{2+}-related spectrum which can be detected at room temperature (RT), and whose intensity is correlated with the sensitivity of the plate.[15,16] While at RT the spectrum can be interpreted as being due to a single type of Eu^{2+} centers with axial symmetry around a <100> axis, below 20 K the spectrum exhibits two contributions due to axial and orthorhombic centers, occurring in a fixed ratio.[17] A detailed electron nuclear double resonance (ENDOR) study revealed the presence of a H_2O (or OH^-) molecule in the close vicinity of the Eu^{2+} ion, and a model was proposed in which a cesium vacancy (V_{Cs}) accounted for the occurrence of two distinct centers at low temperature in a fixed ratio (immobile V_{Cs}) while only one type of centers is observed at high temperature (V_{Cs} bound to the complex, but free to move around it).[18]

Like the PSL properties, also the EPR spectra of NIPs and melt-grown single crystals of CsBr:Eu differ substantially. In previous reports, no Eu^{2+}-related EPR spectra had been

detected in as-grown single crystals,[19] which was attributed to the aggregation of Eu^{2+} ions in CsBr forming diamagnetic pairs or larger clusters. Even earlier, Savel'ev et al.[7] had shown that Eu^{2+} ions in CsBr qualitatively exhibit the same behavior as in the rock-salt type alkali halides : an EPR spectrum exhibiting a hyperfine structure typical for a natural abundant mixture of $^{151}Eu/^{153}Eu$ is produced after quenching the crystals from T > 600 K to 77 K, but it decays at RT following third-order kinetics in the early stage. Hence, the isolated Eu^{2+} centers were assumed to be Eu^{2+}-V_{Cs} dipoles, although, unlike for the centers with a nearest neighbor V_A in the NaCl-type lattices,[6] no angular dependent EPR spectra were presented, specifying the position of the vacancy.

This paper is devoted to a study of the angular dependence of the EPR spectrum of these quenched-in Eu^{2+} centers in CsBr crystals. It is further organized as follows. In Section III.A the EPR spectrum of isolated Eu^{2+} centers in CsBr single crystals is introduced and its limited stability at RT is examined, while in Section III.B the symmetry of the center is determined, resulting in a defect model. The implications for the aggregation mechanism for the Eu^{2+} ions is discussed in Section IV. Sections II and V present experimental details and conclusions, respectively.

II. Experimental

A. Crystal growth and preparation

CsBr:Eu single crystals were grown using the vertical Bridgman technique from CsBr (8.37 g, Sigma-Aldrich, 99.9% purity) and the Eu-dopant Cebla ($CsEuBr_3$, 0.11g). The powders were mixed in a grinder, transferred in a quartz ampoule (6 mm inner diameter) and dried in vacuum at 540 K during 3 days. The evacuated quartz ampoule was fused and heated to 970 K during 4 h before growth (Carbolite two-zone furnace, upper hot zone at 940 K, lower cold zone at 850 K, ampoule lowered at 2 mm/h) in order to obtain a homogeneous melt. After growth, the oven was cooled to RT during 1 day. Undoped crystals grown in this way were clear, transparent and showed no visible evidence of defects (twinning, cracks). The doped crystal was slightly opaque and exhibited a faint yellow color. It had a central inhomogeneity indicating segregation of the dopant. Under UV illumination it exhibited homogeneous blue/purple Eu^{2+}-related luminescence (see figure 1, picture of the crystal in ambient light, under UV excitation, emission spectrum).

Samples of appropriate size for X- (2x2x4 mm^3) and Q-band (1x1x2 mm^3) measurements at microwave frequencies ($\nu_{\mu w}$) of 9.5 and 34.0 GHz, respectively, were cut from the as-grown single crystal using a diamond wire saw and oriented with their long axis parallel to a crystallographic <110> direction by inspection of pole figures on a Bruker D8 θ-θ X-ray diffractometer, with an accuracy of a few degrees. The actual orientation of the samples was determined by fitting the angular dependence of the EPR spectra. The samples were transferred into quartz tubes which were evacuated and sealed. These tubes were annealed

in a preheated oven at 600-840 K typically for 30 min., then quenched to RT or 77 K, and rapidly (within 5 min.) mounted on the EPR sample holders without raising their temperature.

B. EPR measurements and analysis

EPR spectra were recorded in X-band using a Bruker ESP300E EPR spectrometer, with the standard rectangular EPR cavity ER4102ST (TE_{102} mode) fitted to an ESR910 Oxford continuous flow He cryostat, and in Q-band with a Bruker ElexSYS E500 spectrometer with an ENDOR cavity (ER5106QT-E, TE_{013}) and a CF935 continuous flow He cryostat. Field modulation was employed at 100 kHz with an amplitude of 0.3 to 0.5 mT. In order to avoid aggregation of centers[7] during the lengthy recordings of the angular dependence of spectra, these were performed at 20 K and low microwave power (160 μW). The spectra could, however, easily be recorded, with virtually no loss of information, at temperatures up to 80 K and microwave powers of the order of a couple of mW. At RT the spectra exhibit excessive broadening which prevents a detailed angular dependence study, and in addition, the intensity slowly decays.

Spectrum simulations and fittings were performed using the EasySpin routines in Matlab.[20] The usual spin Hamiltonian (SH) for Eu^{2+} centers ($^8S_{7/2}$ ground state, S = 7/2) was used,[21] which for each of the magnetic Eu isotopes (I($^{151/153}$Eu) = 5/2) takes the form

$$\hat{H}_S\left({}^A\mathrm{Eu}\right) = g\mu_B \vec{B}\cdot\hat{\vec{S}} + \sum_{k=2,4,6}\sum_{q=-k}^{k} B_k^q \hat{O}_k^q\left(\hat{\vec{S}}\right) + \hat{\vec{S}}\cdot\vec{A}^A\cdot\hat{\vec{I}}^A \qquad (1)$$

with A = 151,153. The first term in the spin Hamiltonian represents the electronic Zeeman interaction, here assumed to be isotropic, which is a good approximation for S-state ions. The second term parameterizes the Zero Field Splitting (ZFS), with $\hat{O}_k^q\left(\hat{\vec{S}}\right)$ representing the non-normalized extended Stevens operators[20,22] associated with the coefficients B_k^q which are real and given in MHz. The last term represents the hyperfine (HF) interaction of the unpaired electrons with the central Eu nucleus. For simulations the weighed sum of the spectral components corresponding to the two isotopes was calculated, explicitly taking into account the known ratios for the HF constants and natural abundances of the isotopes ($A(^{151}Eu)/A(^{153}Eu) = g_N(^{151}Eu)/g_N(^{153}Eu)$ = 1.3887/0.6130, 47.81 % ^{151}Eu and 52.19 % ^{153}Eu).[23]

III. Results

A. Effect of annealing, quenching and aggregation

In Fig. 2, the EPR spectra of as-grown crystals, stored for a long time in a low humidity environment at RT, and immediately after heating to 840 K and quenching to RT are compared. In both cases the spectra are recorded at RT and at 80 K. It is interesting to note that for crystals annealed to 700 K (or higher) in air, even after rapid quench to RT or 77 K, no EPR spectrum is observed, indicating that during this anneal Eu^{2+} is oxidized to the EPR silent Eu^{3+} state. In line with previous EPR reports[19] on Eu^{2+}-doped CsBr crystals, we do not observe a Eu^{2+}-related signal in as-grown crystals, but a long time after a previous annealing-quenching cycle, the signal in Fig. 2a was recorded at RT. The structure observed in this spectrum can be attributed to HF interaction with the magnetic Eu isotopes.

A sharp line in the spectra (indicated with an asterisk), probably related to an intrinsic defect in CsBr, strongly grows in relative intensity when the recording temperature is lowered from RT to 80 K Fig. 2b. The spectra (a) and (b) exhibit only small variations when the crystal is rotated in the magnetic field. Inspired by previous reports on Eu^{2+} in CsBr[7] and alkali halides of the rock salt type (see Ref. 6 and references therein), we assume this signal is due to aggregated Eu^{2+} in these crystals.

After heating to 840 K for 30 min. and quenching to RT or slightly below (273 K, ice-water temperature) the EPR spectrum recorded at RT (Fig. 2c) still roughly exhibits the same structure (and angular dependence), although the HF pattern is more pronounced. When the sample is kept at RT, the spectrum experiences an important decay in the first few hours and evolves to its stable state (see further in this section). If the spectrum after annealing and quenching is recorded at lower temperature (80 K, here, Fig. 2d), it looks substantially different. It consists of a large number of sharp and intense lines. In this respect, it better resembles the spectra of Eu^{2+} centers observed in the alkali halides of the rock salt type.[6] The twelve central, most intense lines result from the HF split $M_S : -1/2 \rightarrow +1/2$ allowed EPR transition. A detailed study of the angular dependence of the spectrum (Section III.B) demonstrates that all other lines in Fig. 2d belong to the other allowed EPR transitions of the same Eu^{2+} center.

In Fig. 3a selected spectra from the time-evolution at RT of the EPR spectrum after annealing to 840 K and quenching to RT are shown. It is clear that a component exhibiting pronounced HF splitting disappears from the spectra in the first few hours. In Fig. 3b the decay of the signal height at a magnetic field of 1215 mT is presented. In view of the scatter on the data, it is not evident to establish the decay profile in an unambiguous way from the spectral time evolution at a single magnetic field, however. Figure 4 shows the time evolution of the double integrated spectra (total intensity), these allowed the fitting to various decay profiles : exponential decay, pair recombination, recombination by formation of trimers.

These results suggest that in the later stage (after 1500 – 2000 s or 0.5 h) the decay is in a good approximation exponential, with a time constant of about 5500 s (92 min, 1.5 h, see red full line as guide for the eye). There is a marked deviation in the first half an hour, which may simply be the result of an additional fast exponential component. Figs. 4b and 4c, however, indicate that initial recombination in pairs or in triples, may also explain the fast intensity decay immediately after the quench. In this respect the results are in qualitative agreement with those of Savel'ev et al. who proposed trimer formation as primary step in the aggregation of Eu^{2+} ions in CsBr.[7] We assume that the same, or at least very similar, Eu^{2+} centers are involved in our study. The relative contributions of distinct components in the kinetics very probably depend on details of the crystal growth, the doping, and the anneal and quenching.

B. Low temperature spectrum and model of the dominant Eu^{2+} center

To understand the aggregation mechanism of Eu^{2+} ions in CsBr, detailed knowledge of the structure of the Eu^{2+} monomer centers is a prerequisite. In the rock-salt type AX lattices, the model of a nearest-neighbor Eu^{2+}-V_A <110> dipole is well-established from angular dependent EPR measurements.[6] In CsBr a similar <110> dipole was proposed as a model, although in this case this implies that Eu^{2+} and the V_{Cs} occupy next-nearest-neighbor cation positions.[7,24] This identification is to the best of our knowledge not supported by EPR spectral evidence. Even in a more recent EPR study,[25] the proximity of a V_{Cs} to the Eu^{2+} ions is assumed for explaining the aggregation of these ions, but in view of the complexity of the spectra, no definite position for this vacancy is proposed. In fact, it is even suggested that several Eu^{2+} centers with V_{Cs} at different positions contribute to the spectrum.

In Fig. 5 the angular dependences recorded at 20 K in {110} planes for crystals annealed at 840 K during 30 min. and quenched to 77 K, in X- (Fig. 5 a) and Q-band (Fig. 5b) are presented. The angular pattern in the two figures is strikingly similar, and, as demonstrated by simulations, can be completely explained by a single type of cubic centers with S = 7/2. For each magnetic field orientation 7 HF packets of 12 lines (two isotopes with I = 5/2) are in principle expected. The observed number of lines in the spectra is much smaller, on the one hand because the HF packets overlap, and on the other because the outer packets are broadened. In order to reveal the origin of this line broadening, simulations of the <100> spectrum have been performed. The results are summarized in Fig. 6.

Fig. 6a shows the experimental spectrum and that in Fig. 6b is calculated using the SH parameters from Table 1 and a residual line width (full width at half maximum, FWHM) of 0.8 mT. In the experimental spectrum the EPR lines corresponding to the HF packets 1, 2, 6 and 7 are much less pronounced than those for 3, 4 and 5, which is not the case in the simulation 6b. One might consider that the spin of the system is 3/2 rather than 7/2 as an explanation for this remarkable observation, but, in this case cubic ZFS parameters have no

influence on the energy levels and axial parameters B_2^q have to account for the angular dependence of the spectrum. This leads to a lowering of the symmetry of the paramagnetic center and the observation of several symmetry related paramagnetic centers, which were not detected. Simulations of the roadmaps for the center with spin S=3/2 with various B_2^q combinations also demonstrated that the angular dependence of the EPR line positions is completely different in this case.

A more plausible explanation for the broadening of the outer transitions is that, due to a distribution of distant crystal imperfections, a distribution occurs in the ZFS parameters B_k^q. In Figure 6c the simulated EPR spectrum of the cubic Eu^{2+} center is presented taking into account a Gaussian distribution of the B_4^0 parameter with a FWHM of $33\ \mathrm{kHz}$. This simulation already reproduces the experimental spectral line heights and widths much better. The remaining difference between experimental and simulated spectra is most probably caused by the more complex way in which random crystal imperfections affect the ZFS parameters and a distribution of B_2^q and B_6^q may also have to be taken into account. For instance, the deviation between experimental and simulated spectra is even considerably smaller if a Lorentzian distribution in the B_2^0 parameter with maximum at $B_2^0 = 0\ \mathrm{MHz}$ and a FWHM of $4.38\ \mathrm{MHz}$ is applied (Figure 6d). The origin of such a distribution is not clear at this moment, but a distribution of distant lattice defects, e.g. V_{Cs}, presents a plausible explanation.

IV. Discussion : implications for the aggregation mechanism

In view of the earlier reports on Eu^{2+} centers in CsBr, our result that the symmetry of these centers is cubic is highly surprising. Hence we verified that *the same* angular dependence is recorded, without notable appearance of other spectral components, when varying the experimental conditions in the following ways :

1. After subsequent annealing to temperatures up to 300 K
2. When the sample is quenched to 300 K or 273 K instead of to 77 K
3. When the annealing temperature is lower, e.g. 620 K rather than 840 K.

Differences with recently reported results,[25] where relatively low annealing temperatures were applied, are difficult to explain. They might be related with crystal quality (which might lead to additional broadening of the transitions other than $-1/2 \rightarrow +1/2$), annealing atmosphere (not mentioned in Ref. 25, in air Eu^{3+} is produced above 700 K, at lower temperatures maybe other species) or EPR recording temperatures and powers. Concerning the latter, we did, indeed, observe that at 10 K the spectra strongly saturate, even at powers of only a few 100 μW.

In any case, our results demonstrate that the dominant EPR observable monomer Eu^{2+} species in CsBr has cubic symmetry. This either implies that no vacancy is present in the first

few cation shells around the Eu^{2+} ion that would lower the symmetry, or that even at temperatures down to 20 K such a vacancy is so mobile that it freely hops between various neighboring positions around the divalent cation. The latter possibility can practically certainly be excluded, in view of earlier dielectric loss and thermally stimulated current experiments on divalent cation doped CsBr.[26,27] From these experiments activation energies and frequency factors for cation vacancy movement were estimated at ~0.6 eV and ~10^{10} Hz, respectively, implying freeze-out of the vacancy mobility below 200 K. Hence, we conclude that the dominant fraction of isolated Eu^{2+} centers in CsBr has no charge compensating V_{Cs} in its first few surrounding shells.

Although the EPR results strongly indicate that after dispersion Eu^{2+} ions have no V_{Cs} in their direct vicinity, aggregation of these centers at RT (see Section III.A) is hard to imagine if no cation vacancies are involved. Nevertheless, in none of our experiments we could observe centers with lower than cubic symmetry, even when the crystal was annealed for a considerable time to RT, and a notable decay of the Eu^{2+} EPR signal intensity was observed. The detection of centers with V_{Cs} in their direct vicinity may be hampered if the distribution in their ZFS parameters are even larger than for the cubic center, although one would still expect the $-1/2 \rightarrow +1/2$ transition not to be strongly affected by such a distribution. An interesting alternative explanation for these observations is that in the aggregation process the trapping of a V_{Cs} is the rate determining step. This hypothesis implies that after Eu^{2+}_{Cs}-V_{Cs} dipole formation, the migration of such a dipole to others (forming dimers, trimers, clusters or new crystal phases) is virtually instantaneous. Hence, one would expect the activation energy of aggregation to be close to that of V_{Cs} migration through CsBr, although the frequency factor may be largely different. Our attempts to measure the intensity decay of the EPR spectrum as a function of temperature did not allow us to determine the activation energy, though, most probably related to uncertainties in the sample temperature control and measurement.

V. Conclusions

CsBr:Eu single crystals grown from the melt and NIPs differ substantially with respect to Eu^{2+} incorporation. In single crystals isolated Eu^{2+} ions are only produced when aggregates are dispersed at elevated temperature while oxidation is prevented (e.g. by heating in vacuum). They are frozen in by rapidly quenching the crystal to room or lower temperature. At RT the EPR spectrum of Eu^{2+} ions is observed to decay as a result of reaggregation of the ions. In agreement with literature, a fast and a slow component are discerned in this decay. Surprisingly, only Eu^{2+} centers with cubic symmetry were detected with EPR, either suggesting that Eu^{2+}-V_{Cs} dipoles cannot be observed with EPR or that V_{Cs} capture by a substitutional Eu^{2+} ion is the rate-determining step in the aggregation. NIPs, on the other hand, which exhibit a much stronger PSL response to X-ray exposure, have a Eu^{2}-related EPR spectrum with long-term stability at RT. Our earlier EPR and ENDOR studies have shown that

in these centers the Eu^{2+} ion has a H_2O (or OH) molecule in its direct vicinity and most probably also a V_{Cs}. The stability of these centers is most likely a direct consequence of this particular structure.

Acknowledgements

The authors thank prof. D. Poelman and Ing. N. De Roo for their assistance in the making of Fig. 1. H. Vrielinck acknowledges a Postdoctoral Fellowship of the Research Foundation Flanders (FWO-Flanders).

References

[1] M. Nikl, K. Polak, K. Nitsch, G. P. Pazzi, P. Fabeni, and M. Gurioli, Radiat. Eff. Defects Solids **135**, 787 (1995).

[2] R. Aceves,V. Babin, M. Barboza Flores, P. Fabeni, A. Maaroos, M. Nikl, K. Nitsch, G. P. Pazzi, R. Perez Salas, I. Sildos, N. Zazubovich, and S. Zazubovich, J. Lumin. **93**, 27 (2001).

[3] H. F. Symmons and R. C. Kemp, Br. J. Appl. Phys. **17**, 607 (1966).

[4] M. C. M. Delucas, F. Rodriguez, and M. Moreno, Phys. Status Solidi B **172**, 719 (1992).

[5] B. R. Yang, A. Bouwen, and D. Schoemaker, Phys. Status Solidi B **127**, 657 (1985).

[6] J. Rubio, J. Phys. Chem. Solids **52**, 101 (1991).

[7] V. P. Savel'ev, V. P. Avdonin, L. D. Dugarova, A. P. Nedashkovskii, and B. T. Plachenov, Fiz Tverd Tela+ **16**, 1090 (1974).

[8] J. H. Crawford, J. Phys. Chem. Solids **31**, 399 (1970).

[9] M. Zdravkova, H. Vrielinck, F. Callens, E. Boesman, H. Vercammen, and D. Schoemaker, J. Appl. Phys. **82**, 2476 (1997).

[10] M. T. Barriuso, P. Garcia-Fernandez, J. A. Aramburu, and M. Moreno, Solid State Commun. **120**, 1 (2001).

[11] H. Vrielinck, K. Sabbe, F. Callens, P. Matthys, and D. Vandenbroucke, Spectrochim. Acta A **56**, 319 (2000).

[12] P. Leblans, D. Vandenbroucke, and P. Willems, Materials **4**, 1034 (2011).

[13] P. J. R. Leblans, L. Struye, and P. Willems, P Soc Photo-Opt Ins **2**, 59 (2001).

[14] N. M. Winch and A. Edgar, Nucl. Instrum. Meth. A **654**, 308 (2011).

[15] F. Loncke, H. Vrielinck, P. Matthys, F. Callens, J. P. Tahon, and P. Leblans, Spectrochim. Acta A **69**, 1322 (2008).

[16] F. Loncke, H. Vrielinck, P. Matthys, F. Callens, J. P. Tahon, and P. Leblans, Appl. Phys. Lett. **92**, Art. no. 204102 (2008).

[17] F. Loncke, H. Vrielinck, P. Matthys, F. Callens, J. P. Tahon, P. Leblans, I. Ahmad, and E. Goovaerts, Phys. Rev. B **79**, Art. no. 174102 (2009).

[18] H. Vrielinck, F. Loncke, J. P. Tahon, P. Leblans, P. Matthys, and F. Callens, Phys. Rev. B **83**, Art. no. 054102 (2011).

[19] S. Schweizer, U. Rogulis, S. Assmann, and J. M. Spaeth, Radiat. Meas. **33**, 483 (2001).

[20] S. Stoll and A. Schweiger, J. Magn. Reson. **178**, 42 (2006).

[21] A. Abragam and B. Bleaney, *Electron paramagnetic resonance of transition ions* (Clarendon Press, Oxford, 1970).

[22] C. Rudowicz and C. Y. Chung, J. Phys. Condens. Matter **16**, 5825 (2004).

[23] *Bruker Biospin Almanac* (Bruker Analytik GmbH, Rheistetten, 2010), p. 47.

[24] F. Loncke, *Magnetic resonance study of dopant related defects in X-ray storage phosphors*, Ph.D. thesis, Ghent University, 2009.

[25] D. O. Tolmachev, A. G. Badalyan, R. A. Babunts, V. A. Khramtsov, N. G. Romanov, P. G. Baranov, and V. V. Dyakonov, J. Phys. Condens. Matter **22** (2010).

[26] S. Radhakrishna and S. Haridoss, Journal De Physique **38**, 841 (1977).

[27] S. Radhakrishna and K. P. Pande, Phys. Rev. B **7**, 424 (1973).

FIGURES

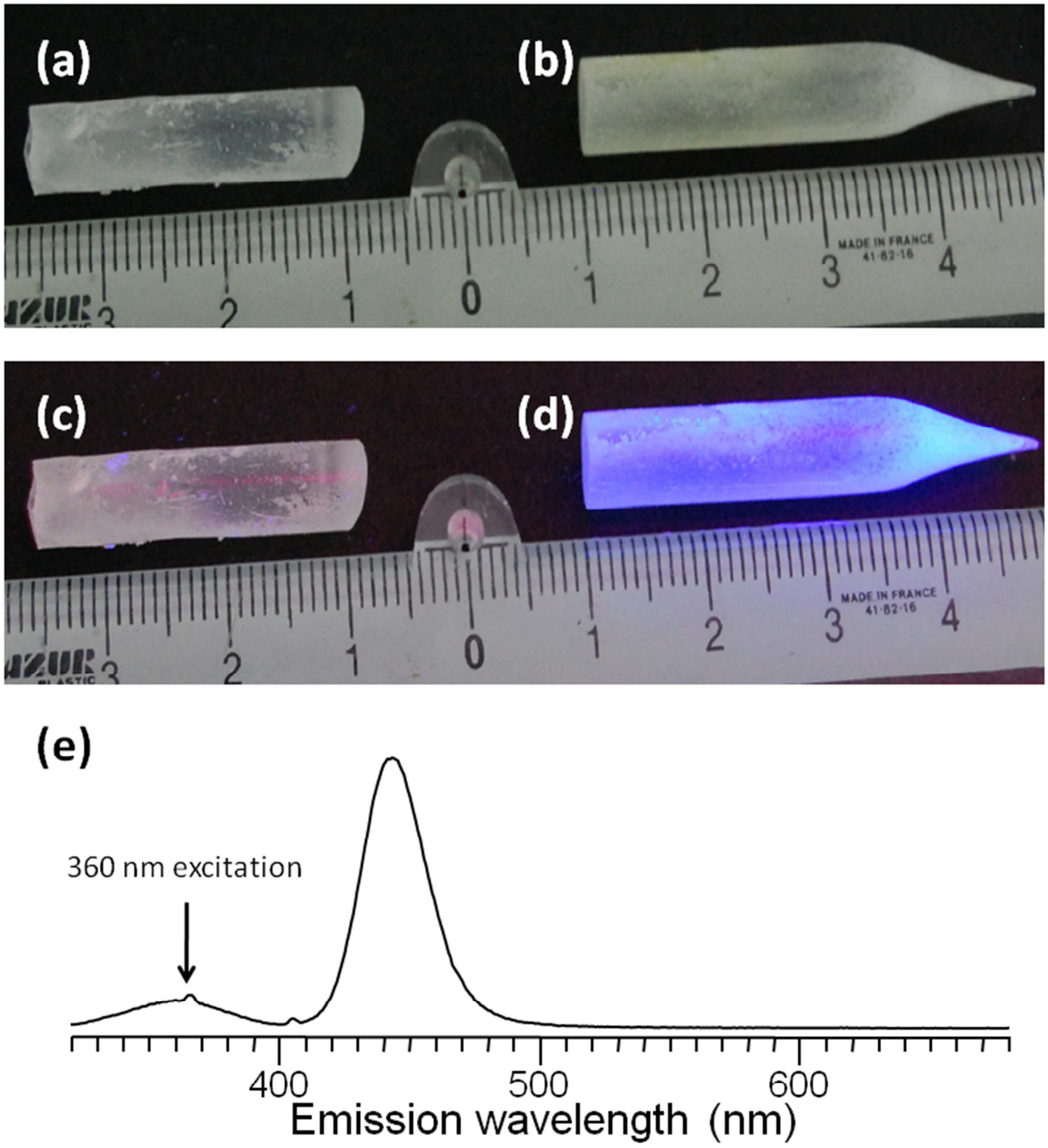

Figure 1 : *Undoped (a,c) and Eu^{2+} doped (b,d) melt-grown CsBr crystals under ambient (a,b) and UV (c,d) light, (e) emission spectrum of the CsBr:Eu^{2+} crystal under UV (360 nm) excitation.*

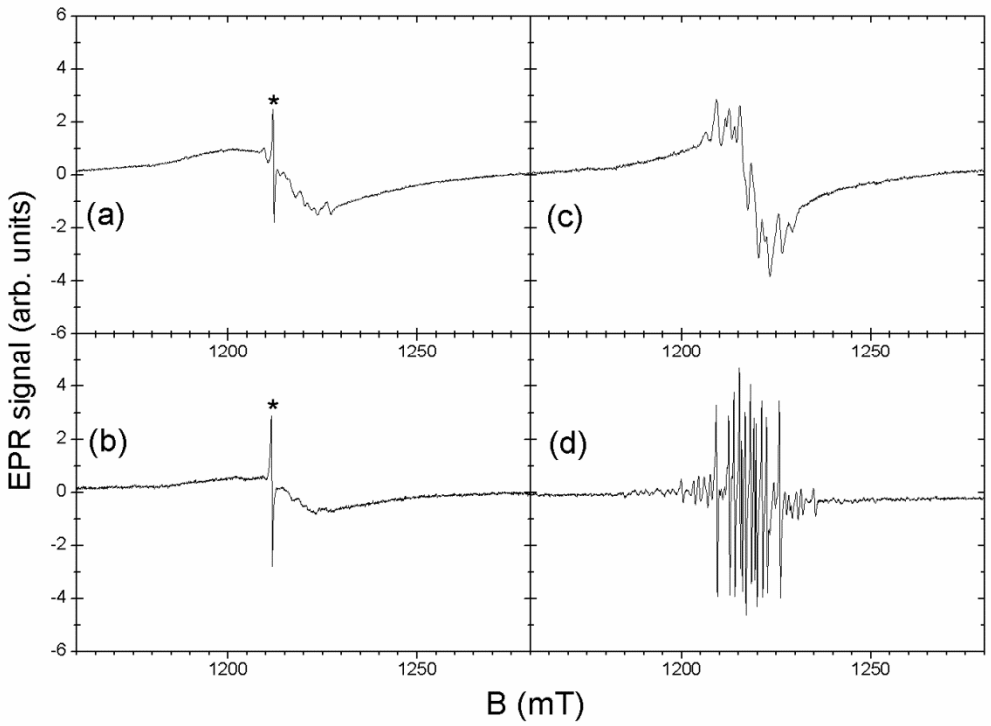

Figure 2 : *Q-band EPR spectra of (a,b) CsBr:Eu^{2+} crystals stored for a long time at RT and (c,d), a short time after heating to 840 K and quenching to 273 K. Spectra (a,c) are recorded at 265 K and (b,d) at 80 K. The line marked with an asterisk is not (directly) related to Eu^{2+} ions.*

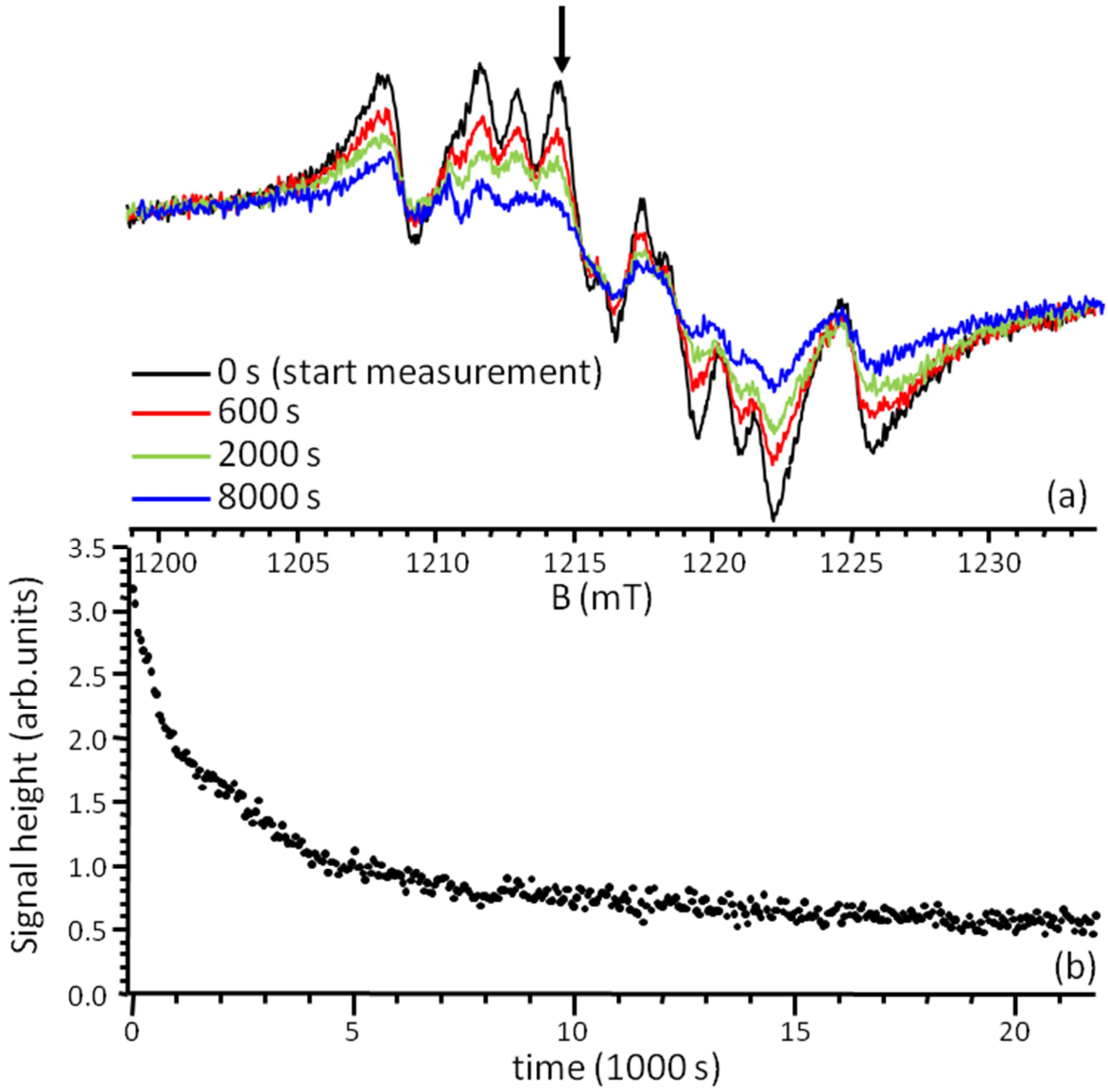

Figure 3 : *Decay at RT of the intensity of the cubic Eu^{2+} Q-band EPR spectrum in melt-grown CsBr:Eu single crystals, after heating to 840 K and quenching to RT. (a) Selected EPR spectra recorded at different times after quench (measurement starts approximately 300 s after the quench. (b) Time-dependence of the signal height at B = 1215 mT, marked with an arrow in (a).*

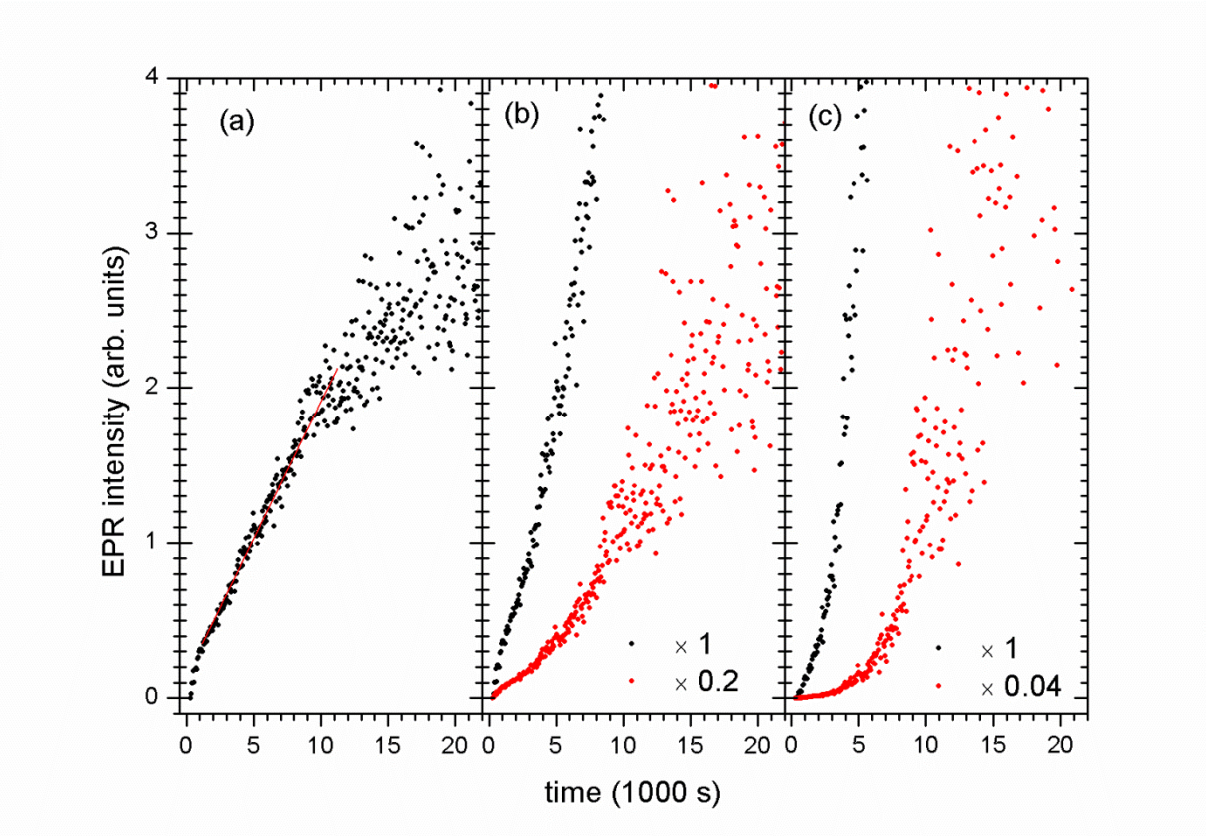

Figure 4 : *Representations of the time evolution of the total intensity (I(t)) of the EPR spectrum of isolated Eu^{2+} in CsBr (intensity of last spectrum in the time evolution subtracted) after heating to 840 K and quenching to RT, for testing various decay models.*

(a) $\ln\left(I(0)/I(t)\right)$ *: exponential decay modeled by* $dI(t)/dt = -\alpha I(t)$

(b) $\left(I(0)/I(t)\right)-1$ *: decay by pair formation modeled by* $dI(t)/dt = -\alpha I^2(t)$

(c) $\left(I(0)/I(t)\right)^2-1$ *: decay by trimer formation modeled by* $dI(t)/dt = -\alpha I^3(t)$

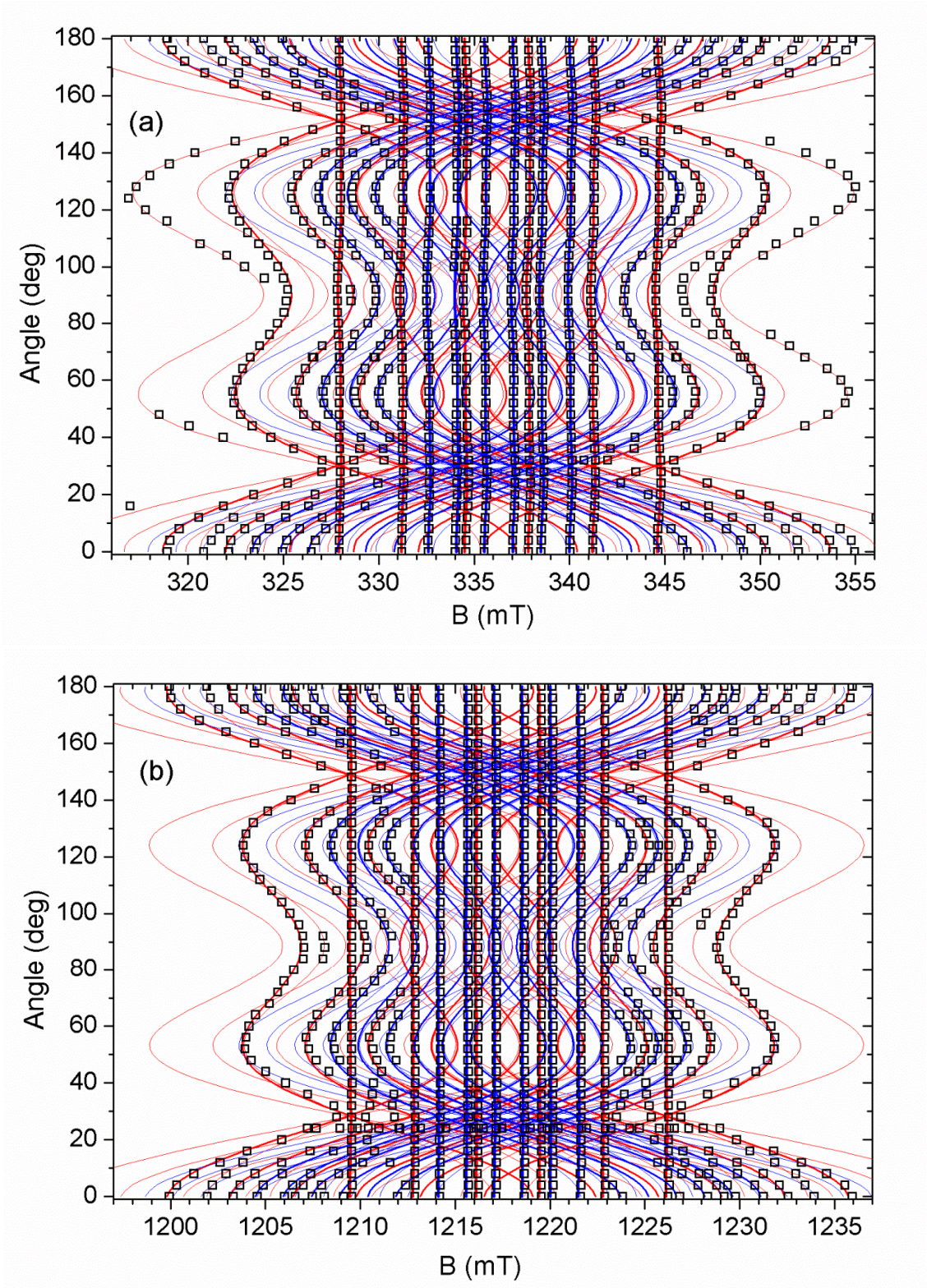

Figure 5 : *Angular dependence of the EPR spectrum, recorded at 20 K, of the dominant, cubic Eu^{2+} center produced in melt-grown CsBr:Eu single crystals by heating to 770-840 K and quenching the crystal to 300 K or 77 K, (a) in X-band (9.57 GHz) and; (b) in Q-band (33.99 GHz). Open square symbols represent experimental resonance positions and full lines simulations for the two Eu isotopes (red ^{151}Eu, blue ^{153}Eu), using the spin Hamiltonian parameters in Table 1.*

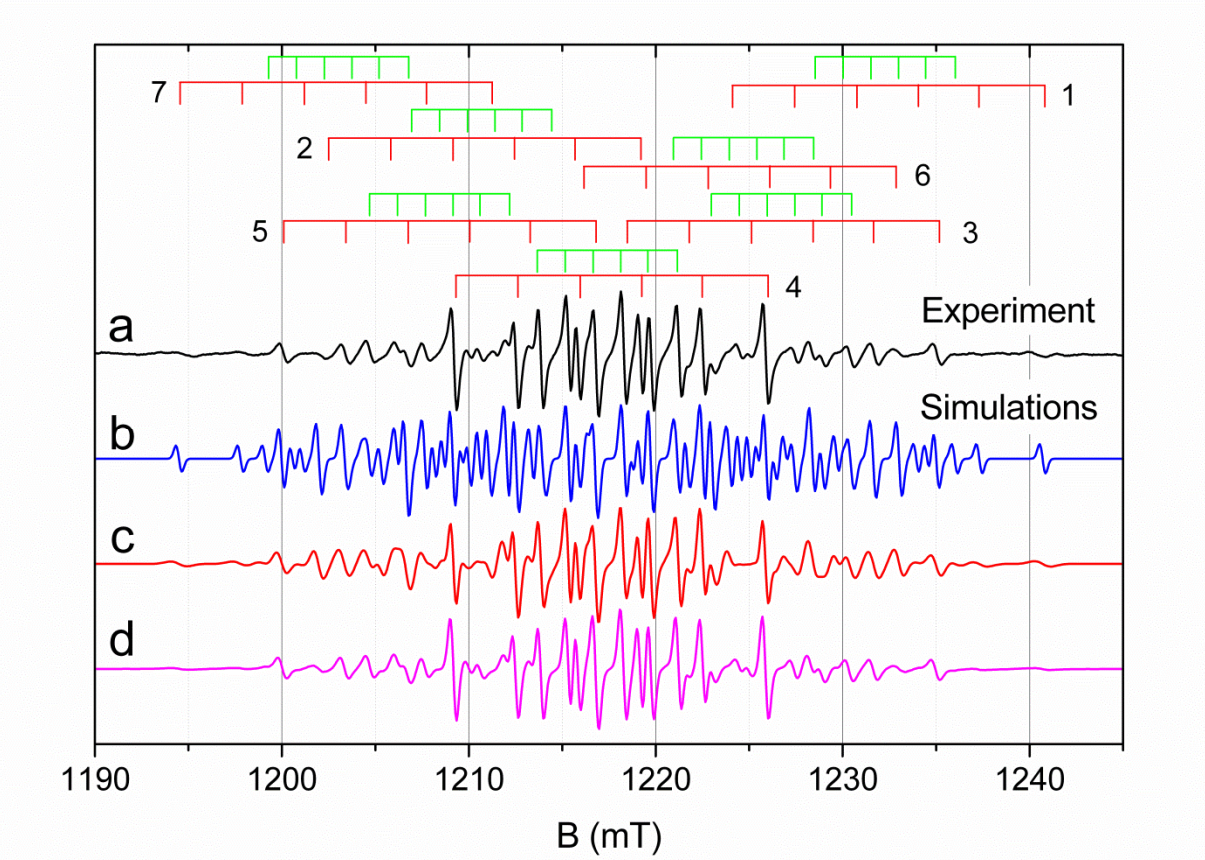

Figure 6 : *Experimental EPR spectrum and simulations of the cubic Eu^{2+} spectrum produced in melt-grown CsBr:Eu single crystals by heating to 840 K and quenching the crystal to 77 K. (a) Q-band spectrum recorded at 80K in the <100> orientation and at $\nu_{\mu w}$ = 33.98 GHz. (b) Simulated spectrum of cubic Eu^{2+} without distribution in the ZFS parameters. (c) and (d) Same as (b) but with a Gaussian distribution in B_4^0 around $363\ kHz$ with $FWHM = 33\ kHz$ and a Lorentzian distribution in B_2^0 around 0 MHz with $FWHM = 4.38\ MHz$, respectively. The labeling of the transitions is as follows :* ***1****: -7/2 → -5/2,* ***2****: -5/2 → -3/2,* ***3****: -3/2 → -1/2,* ***4****: -1/2 → +1/2,* ***5****: +1/2 → +3/2,* ***6****: +3/2 → +5/2,* ***7****: +5/2 → +7/2.*

Table 1 : *Spin Hamiltonian parameters for the cubic Eu^{2+} center produced in melt-grown CsBr:Eu single crystals by heating to 770-840 K and quenching the crystal to 300 K or 77 K, determined by fitting the angular dependence of the EPR spectra recorded at 20 K. Subscripts indicate the error in the least significant digit.*

g (dimensionless)	1.993_1
A(^{151}Eu) (MHz)	-92.9_2
$\mathbf{B_4^0}$ (MHz)	0.363_6
$\mathbf{B_6^0}$ (kHz)	-0.44_2